Available online at www.sciencedirect.com

ScienceDirect

Ceramics International 40 (2014) 2365–2372

CERAMICS INTERNATIONAL

www.elsevier.com/locate/ceramint

Photocatalytic activity of visible-light-active iron-doped coatings prepared by plasma spraying

P. Ctibor[a,*], Z. Pala[a], V. Stengl[b], R. Musalek[a]

[a]Institute of Plasma Physics, ASCR, Za Slovankou 3, 182 00 Praha 8, Czech Republic
[b]Institute of Inorganic Chemistry, ASCR, 250 68 Husinec-Rez, Czech Republic

Received 27 May 2013; received in revised form 29 July 2013; accepted 1 August 2013
Available online 9 August 2013

Abstract

This study examines the photocatalytic activity of coatings produced by atmospheric plasma spraying (APS). The applied spraying tools were gas-stabilized (GSP) and water-stabilized (WSP) plasma guns. The TiO_2–Fe_2O_3 powder with and without Na_2SiO_3 additive was produced as agglomerates suitable for feeding into the plasma jet. The coatings are analyzed by scanning electron microscopy, X-ray fluorescence and X-ray diffraction. Photocatalytic degradation of butane under UV and under visible light, as well as the growth kinetics of the products – carbon dioxide and carbon monoxide – is quantified for all coatings and compared with a pure TiO_2 coating. The coatings show a lamellar structure, as it is typical for this process. However, their porosity is rather high. Anatase titania from the feedstock powder is converted into rutile phase in all coatings; whereas the presence of $FeTiO_3$ is detected in the coating without Na_2SiO_3 made by WSP and metallic iron in the GSP coating. The coating from powder with Na_2SiO_3 admixture is partly amorphous. This coating is photocatalytically active especially under UV, whereas under visible light it is overcome by the WSP coating. The GSP coating has the best photocatalytic activity under both different radiations.

Keywords: B. Spectroscopy; Band gap; Plasma spraying; Photocatalysis; TiO_2–Fe_2O_3

1. Introduction

When TiO_2 is illuminated by photons having energy higher than TiO_2 band gap, charge carriers are photogenerated promoting oxidation and reduction reactions. This photocatalytic activity is applied, for example, in water purification [1,2] and air cleaning [3]. The photocatalytic activity of the coatings can vary with the composition, stoichiometry, hydroxyl and impurity concentrations, porosity, surface roughness as well as with the micro- or nano-structure [4]. Another influential factor on the photocatalytic activity is, of course, the phase composition of the material. There is a demand for fabrication techniques of TiO_x films, in both crystalline as well as amorphous state, and coatings applicable to a large area deposition and high quality coverings achieved even at low substrate temperatures [5].

A search for methods of improvement of the photocatalytic efficiency of the TiO_2-based coatings is a desirable subject of research and development. It has also been realized that the band gap of anatase TiO_2, which is about 3.2 eV, means that the electron can only be excited by the high-power UV light irradiation with a wavelength shorter than 387 nm [6]. A multiple band gap photocatalytic reaction cell was formed in composite TiO_2–Fe_3O_4 coatings [7]. Part of the material reacts in plasma according to the following formula:

$$Fe_3O_4+TiO_2 \rightarrow FeTiO_3+Fe_2O_3 \quad (1)$$

$FeTiO_3$, as a p-type semiconductor with a band gap about 2.5 eV, is advantageously combined with a sub-stoichiometric TiO_2, which is n-type semiconductor, thus, a solid p–n junction formation in the sprayed coating is possible [8]. The TiO_2–Fe_3O_4 coatings consisted of anatase TiO_2, rutile TiO_2 and pseudobrookite Fe_2TiO_5 phase which appeared when the content of Fe_3O_4 additive was over 10 wt% [6]. Relatively low addition of Fe_3O_4 led to occurrence of ilmenite $FeTiO_3$ phase in the coatings. The content of anatase in the sprayed coatings decreased with the increasing Fe_3O_4 content. The photocatalytic activity was improved by an increase of $FeTiO_3$ content in the coating, which was explained by good photoabsorbance and by the two-step electron transfer model [6].

*Corresponding author. Tel.: +420 266053717; fax: +420 28586389.
E-mail address: ctibor@ipp.cas.cz (P. Ctibor).

0272-8842/$ - see front matter © 2013 Elsevier Ltd and Techna Group S.r.l. All rights reserved.
http://dx.doi.org/10.1016/j.ceramint.2013.08.007

During the photocatalytic reactions, when a semiconductor containing TiO_2 and $FeTiO_3$ is UV-irradiated, the electron–hole pairs possibly form in two steps [8]. In the first step the electron is initiated from the valence band to the conduction band of $FeTiO_3$, and in the second step the electron in the conduction band of $FeTiO_3$ is initiated to the conduction band of TiO_2. The benefit, called also inter-semiconductor hole-transfer mechanism [9], is an extension of the light absorption range and the possible recombination of the excited holes and electrons.

The plasma sprayed TiO_2 is typically slightly sub-stoichiometric (TiO_{2-x}) [10,11] and we propose the use of Fe_2O_3 instead of Fe_3O_4 in order to avoid this phenomenon. In this case, part of the material will follow the reaction (2), especially when using a high-temperature jet of the water-stabilized plasma gun [12] available for our spray tests.

$$Fe_2O_3+2TiO_2 \rightarrow FeTiO_3+TiO+FeO+O_2 \quad (2)$$

The free oxygen, released according to the formula (2), can replace the oxygen deficiency in TiO_{2-x} resulting from the reducing environment of the plasma jet. The FeO evaporates preferentially because of its melting point at 1370 °C which is about 180 °C lower than melting points, and simultaneously decomposition points, of both Fe_2O_3 and Fe_3O_4 at 1550 °C. TiO is created in a small amount only.

The goal of the present paper is to examine the influence of two plasma spray processes by APS on the composition, microstructure and photocatalytic activity of TiO_2 powder doped with Fe according to the above described considerations.

2. Experimental

2.1. Powder synthesis

An original technique was used for preparation of the TiO_2–Fe_2O_3 composition. Ten liters of 1.6 M solution $TiOSO_4$ (99.9% purity; Sigma-Aldrich) was diluted in 60 l of water. Then 1.6 kg of $FeSO_4$ (99.0% purity; Sigma-Aldrich) and 6 kg of urea were added. The reactive mixture was boiled at 98 °C for 8 h, decanted, filtered and dried at 105 °C. This method is based on thermal decomposition of urea at a temperature higher than 60 °C. The products of these reactions are mostly spherical agglomerates composed of sub-micrometric individual spheres.

After drying, disintegration of dry TiO_2–Fe_2O_3 large agglomerates and sieving we obtained a feedstock with sizes 63–125 μm and 20–63 μm for the WSP and GSP spray processes respectively. The size distribution for each process is dictated by the plasma temperature at the powder feeding point. The powder must be properly melted but evaporation should be minimized for good effectivness of the process. This feedstock is further labeled FeT and contains TiO_2 with nominally 5 wt% of Fe_2O_3. However, a majority of the powder disintegrated during sieving back to very fine particles, unsuitable for plasma spraying. We searched for an easy re-agglomeration process using an inorganic substance which can be released at a thermal processing. The ideal candidate would be a substance enhancing structural features that would promote the photoactivity as well. We have chosen Na_2SiO_3, because it can influence the surface state and phase transformations of TiO_2 [13,14]. The mixture was prepared mechanically with 1:1 ratio of the disintegrated "FeT" fine powder with so called "water glass", which contained 38 wt% of Na_2SiO_3 whereas the rest is silicic acid, and dried the resulting product at a room temperature. After careful crushing and further sieving, we obtained a feedstock for the WSP spray process, with the size 63–125 μm. The phase composition of this feedstock is shown in the results section.

2.2. Spray processes

The plasma gun used for GSP spraying was a gas-stabilized plasma gun based on Ar+H_2 mixture as a plasma-forming gas. The parameters used were: Plasma gas Ar+H_2 (9+10 slpm); Spray distance (SD) 150 mm; Torch current 650 A and voltage 58 V; Powder feeding gas–argon (flow rate 3.2 slpm). Powder feed rate was set to 2–5 kg/h and substrates were made from stainless steel, $120 \times 25 \times 3.5$ mm^3. The substrates were grit blasted and acetone degreased before the spraying. The resulting coating is labeled FeT–GSP.

Another plasma gun used for spraying was a water-stabilized plasma gun (WSP) working with a dc-current and water vapor as a plasma-forming gas. The parameters used were: Feeding distance (FD) 105 mm; Spray distance (SD) 350 mm; Torch current 480 A and voltage 320 V; Powder feeding gas–air (flow rate 3.25 slpm). Powder feed rate was set to 12–15 kg/h and substrates were the same as for GSP. The resulting coatings are labeled FeT-WSP and FeT-WSP–VS (from powder with Na_2SiO_3).

As the reference sample "*R*" for the photocatalytic test at 365 nm, anatase layer (described [15] as prepared without surfactants and denoted "TIT300" in [15]) was concerned. For preparing this sample mesoporous titania (anatase) powder was dispersed in a 1:1 volumetric mixture of poly-hydroxyethyl methacrylate and ethanol. From this suspension, a 300 μm thin layer was created on a glass desk. The general difficulty to prepare anatase coating by any available thermal spray technique forced us to use this sample with a completely different microstructural characters [15].

2.3. Characterization techniques

X-ray diffraction (XRD) was performed on a D8 Discover Bruker theta–theta Bragg-Brentano diffractometer using CuKα radiation and 1D LynxEye detector. The obtained diffraction patterns provided information not only about the phase composition of feedstock powders and coatings, but also about the corresponding grain sizes. The size of crystallites is represented by domains of coherent scattering which was calculated according to two approaches – for rutile we used the Williamson–Hall graph and the Scherrer formula for {101} anatase diffraction peak. The influence of the instrumental broadening was taken into account by measuring calcium fluoride standard.

Raman spectroscopy was performed using Lambda Solutions P1 apparatus with laser wavelength of 785 nm, objective magnification 50 × and 25 s integration time. The surface of the coating was polished before the test.

Porosity of the coatings was measured by image analysis of cross-sectional micrographs taken with a CCD camera. For analysis of light micrographs the software Lucia G (Laboratory Imaging, Czech Rep.) was used. Reported values are averages from 10 frames analyzed at 250 × magnification. In addition to the simple quantification of porosity, other factors of the voids were also examined. Circularity of pores (planar 2D projections) is equal to zero for a line and to 1 for a circle. Plasma sprayed coatings contain typically pores flattened parallelly with the surface as a result of the lamellae (so called splat) formation.

The surface roughness was recorded by the Surtronic 3P (Taylor Hobson, UK) using the contact technique. Microhardness was measured by a Hanemann microhardness head (Zeiss, Germany) mounted on an optical microscope with a fixed load of 1 N and a Vickers indenter. Twenty indentations from various areas of a cross section for each sample were analyzed.

Morphological observations of the as-sprayed surfaces of selected coatings were performed in an EVO MA15 scanning electron microscope – SEM (Carl Zeiss, Germany) in back-scattered and/or secondary electron modes.

The reflectance measurement in this work was implemented using ultra-violet/visible/near-infrared (UV/Vis/NIR) spectrophotometer (Shimadzu, Japan). Prior to the actual measurement, the calibration process was conducted using the $BaSO_4$ reference mirror in order to minimize the error from environment. The accuracy guaranteed by the equipment manufacturer is that of the wavelength ± 0.3 nm and the uncertainty of the measurement less than 0.2%. The wavelength of incident light used for the reflectance measurement was in the range from 250 to 2000 nm, and the diameter of the measured area was about 2 cm^2. The corresponding band gap energy was estimated after converting the reflectance curves to absorbance and recalculation [16] to Kubelka–Munk absorbance units.

Kinetics of the photocatalytic degradation of butane (0.87%) was measured by using a home-made stainless steel batch photoreactor [17] with a Narva black-light fluorescent lamp at the wavelength of 365 nm and warm white fluorescent lamp at the wavelength of up to 400 nm (input power 8 W, light intensity 6.3 mW cm^{-2}). Gas concentration was measured with the use of a quadrupole mass spectrometer JEOL JMS-Q100GC and a gas chromatograph Agilent 6890N. A high-resolution gas chromatography column (19091P-QO4, J&W Scientific) was used. The sample from the reactor was taken via a sampling valve at time intervals of 2 h. The reactor with the total volume of 3.5 l was filled with oxygen by 1 l per minute flow rate. Blank tests – a layer of poly(hydroxyethyl methacrylate) without titania – were performed to establish the effect of photolysis and catalysis on the conversion of butane. The UV irradiation test without any photocatalyst detects that there was no or immeasurable conversion of butane, as a testing gas, into CO and/or CO_2 and consequently butane was also not adsorbed on the poly(hydroxyethyl methacrylate) matrix. The injection volume of butane into the photoreactor was 30 ml.

3. Results and discussion

3.1. Microstructure and phase composition

Light micrographs of the coatings FeT-WSP and FeT-WSP–VS are shown in Fig. 1. The cross section of the FeT-WSP coating shows a rather porous lamellar microstructure. The FeT-WSP–VS coating is displayed in an in-plane view because the integrity of the coating was rather low and preparation of a well polished cross section was not possible. We can see predominantly circular pores with various sizes of up to 50 μm. The FeT-GSP coating was too thin for preparation a cross section and for in-plane polishing as well; taking into account the surface roughness induced on the steel substrate by the grit blasting prior to spraying, the contiguous covering will be lost when GSP coating is polished.

A SEM micrograph of the surface of the FeT-WSP coating is displayed in the Fig. 2a. The surface contains a lot of globular particles approximately from 1 to 5 μm in diameter. These particles originate from larger agglomerated units, disintegrated in the plasma jet, which solidified probably before impact onto small globular particles adhering only chemically on the coating surface. The feedstock powder FeT was rather irregular with fine particles adhering on the surface only with a limited compactness [18]. The FeT-WSP coating surface, Fig. 2a, does not show any pronounced flattening into

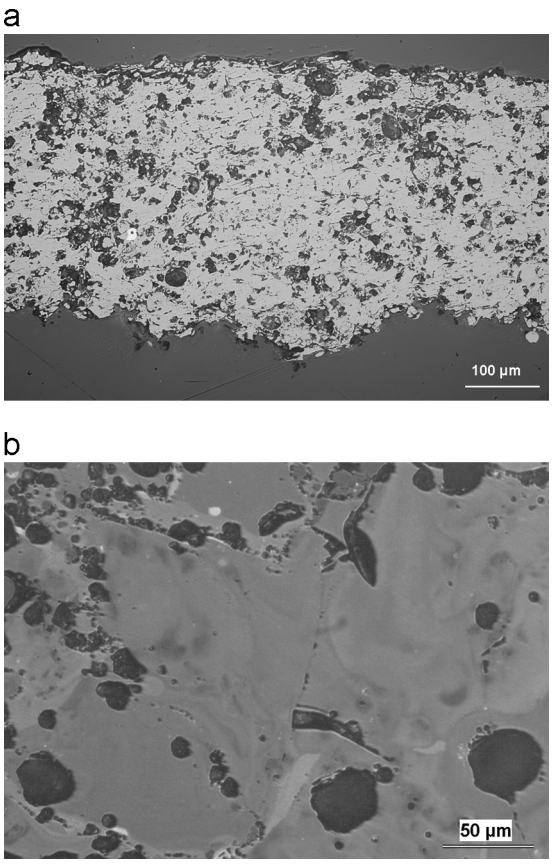

Fig. 1. (a) FeT-WSP, light micrograph of the cross section of the plasma sprayed coating. (b) FeT-WSP–VS, light micrograph of the in-plane section of the plasma sprayed coating.

lamellae and mechanical anchoring to previous layers. For such a microstructure we can preclude a low mechanical integrity of the entire coating. However, the cross section, Fig. 1a, shows a partly lamellar microstructure quite typical for a plasma sprayed coating, only with relatively high porosity. A SEM micrograph of the surface of the FeT-GSP coating, Fig. 2b, presents a sponge-like structure with many open craters from approximately 15 μm in diameter down to a scale under 1 μm.

The feedstock powders, especially the FeT-VS powder, were relatively soft and needed to be handled with care to prevent disintegration before feeding into plasma. The spray process efficiency of such powder cannot be expected as very high and the porosity is a consequence of it. But for a photocatalytic application the large area available for interaction between light, the catalyst and the decomposed pollutant is an advantage.

The results of phase analyses are summarized in Table 1 Phase composition of the FeT-VS feedstock powder is: anatase TiO_2, hematite Fe_2O_3 and ammonium sulfate $(NH_4)_2SO_4$ (mascagnite). Sulfur in the ammonium sulfate phase originates from unreacted $TiOSO_4$ used at TiO_2 production or unreacted $FeSO_4$ from Fe_2O_3 production. The FeT feedstock, Fig. 3, contained anatase (85 wt%), hematite Fe_2O_3 (6%) and amonium sulfate $(NH_4)_2SO_4$ (9%), and was completely crystalline as well as the FeT-WSP coating, which contained 84 wt% of rutile, 3% of anatase and 13% of ilmenite $FeTiO_3$. However, significant presence of amorphous material in both FeT-WSP–VS and FeT-GSP coatings was observed in XRD patterns. Quantitative Rietveld refinement of XRD patterns of the irradiated volume yielded within the crystalline material the following weight percentages, 78 wt% of rutile and 22% of anatase in the FeT-WSP–VS coating. The FeT-GSP coating contained 36% of rutile, 17% of anatase, 38% of austenite (f.c.c. Fe) and 10% of ferrite (b.c.c. Fe).

Na_2SiO_3 in the FeT-WSP–VS coating suppresses partly the anatase to rutile phase transformation. Ilmenite was created during spraying and quenching from iron oxide phases and titania, similarly as in the literature [6–8]. The metallic iron detected in FeT-GSP coating is a product of reduction of iron oxides in the hydrogen-rich atmosphere of the GSP process. The percentage of both Fe phases is high because Fe is fully crystalline, which is not the case of the resting material (containing preferably other elements).

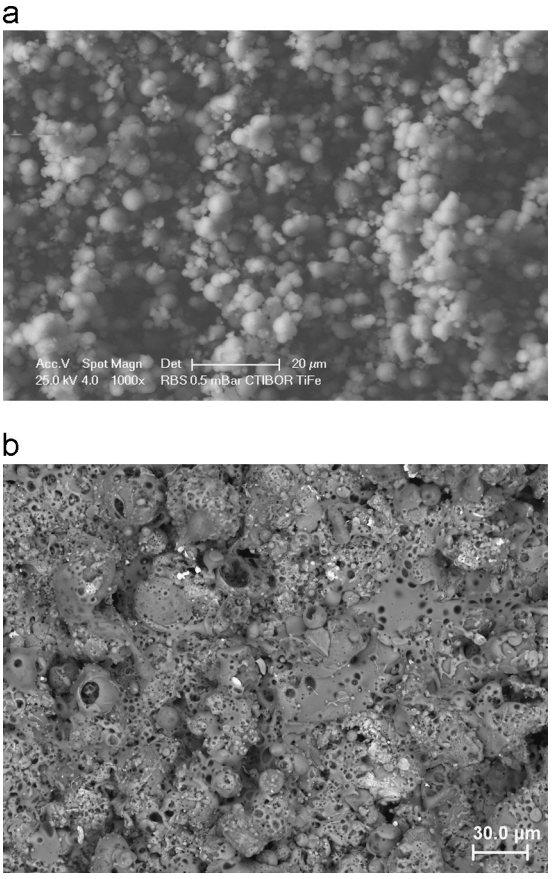

Fig. 2. (a) surface of the FeT-WSP plasma sprayed coating, SEM-SE. (b) Surface of the FeT-GSP plasma sprayed coating, SEM-BE.

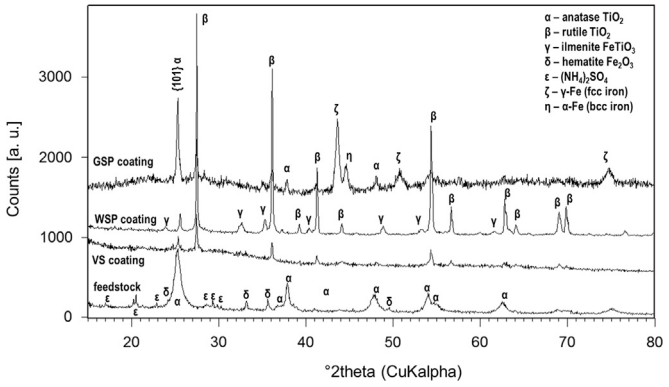

Fig. 3. XRD patterns of the FeT-VS feedstock powder, FeT-WSP coating, FeT-WSP–VS ("VS coating") and FeT-GSP coating.

Table 1
Results of Rietveld refinement of XRD patterns in wt% of the crystalline material; when the refinement was not successful, only YES or NO indicate the qualitative results.

Sample	**Anatase TiO_2**	**Rutile TiO_2**	**Hematite Fe_2O_3**	**Ilmenite $FeTiO_3$**	**Austenite f.c.c. Fe**	**Ferrite b.c.c.Fe**	**$(NH_4)_2SO_4$**
FeT feedstock	85	No	6	No	No	No	9
FeT-VS feedstock	Yes	No	Yes	No	No	No	Yes
FeT-WSP coating	3	84	No	13	No	No	No
FeT-WSP–VS coating	22	78	No	No	No	No	No
FeT-GSP coating	17	35	No	No	38	10	No

The average size of anatase crystallites is 12 nm for the FeT feedstock, 39 nm for the FeT-GSP coating, 69 nm for the FeT-WSP coating, and 81 nm for the FeT-WSP–VS coating. For the reference *R* sample it is 30 nm [15]. The average size of rutile crystallites was similar for the FeT feedstock and FeT-WSP coating – about 150 nm. For the FeT-WSP–VS coating it is 190 nm and 680 nm for FeT-GSP coating. Hence, the FeT-GSP coating has the coarsest rutile but the finest anatase crystallites among all coatings. Its thickness was the smallest and microstructure very porous, so its cooling was relatively fast and the low-temperature phase (anatase) has not enough time for crystallite growth. In the coating FeT-WSP–VS the Na_2SiO_3 component contributes to amorphization by blocking the crystallite nucleation.

Average porosity of the FeT-WSP coating is 28%, whereas mean equivalent diameter of pores is 17.6 μm and the maximum equivalent diameter of pores is 42.4 μm. Minimal circularity of pores is 0.041. This means that FeT-WSP coating is very porous, the voids are large and non-globular (indication of well flattened lamellae). The FeT-WSP–VS coating with its low integrity restricted proper image analysis.

Table 2 shows XRF analysis of the FeT-WSP coating. The atomic ratio Ti/Fe is 4.08. Table 3 summarizes surface roughness of the FeT-WSP and FeT-WSP–VS coatings. We can see the high roughness of the FeT-WSP–VS coating from the viewpoint of both parameters, whereas the FeT-WSP coating has also markedly coarser surface than the FeT-GSP coating.

Microhardness of the FeT-WSP coating is 8.7 ± 1.6 GPa, whereas FeT-WSP–VS coating is softer with 6.8 ± 1.0 GPa. The reference coating *R* is even softer; due to plastic binder non-measurable by instrumentation of the Hanemann type (a depth-sensing technique – probably more promising – was not used). As mentioned earlier, the FeT-WSP–VS coating did now allow the cross-sectional cut, and therefore its hardness was measured in the in-plane section.

Table 2
XRF analysis of the FeT-WSP coating.

Element	Wt%	At%
O (K)	41.79	68.94
Ti (K)	45.26	24.94
Fe (K)	12.94	6.12
Total	100.00	100.00

Raman spectra are displayed in Fig. 4. On the spectrogram of the FeT-WSP coating, an anatase peak at 399 cm^{-1} and a rutile peak at 440 cm^{-1} are present as well as one wider peak centered at about 420 cm^{-1}. This same feature, however much less pronounced, is presented also on the spectrum of the FeT-WSP–VS coating. The position of the rutile peak located at about 445 cm^{-1} shifts to low wavenumbers as the O/Ti ratio starts to decrease [19,20]. An incorporation of Fe^{3+} into TiO_2 creates large amounts of oxygen vacancies, and due to them, the E_g peak of rutile phase located around 445 cm^{-1} at zero concentration of iron ions shifts to the low wavenumbers with an increase in iron content [19]. Raman line shift and broadening correspond to thermal treatment in the air and are therefore attributed to an oxygen deficiency effect [21]. The FeT-WSP coating also has one rutile peak at 610 cm^{-1}. For the FeT-WSP–VS coating, this peak is not clear enough because of partly amorphous composition. All three coatings have the anatase peak at 144 cm^{-1}, however, not very intensive.

3.2. Opto-electric properties

Energy of the transfer of an electron from the valence band to the conduction band is expressed in Fig. 5 in Kubelka–Munk absorbance units (KMU) [22]. The Kubelka–Munk intensity for the FeT-WSP coating as well as FeT-GSP coating, which is approximately 7 KMU at the UV light wavelength of 365 nm, are both lower than 9 KMU of the FeT-WSP–VS coating. At the

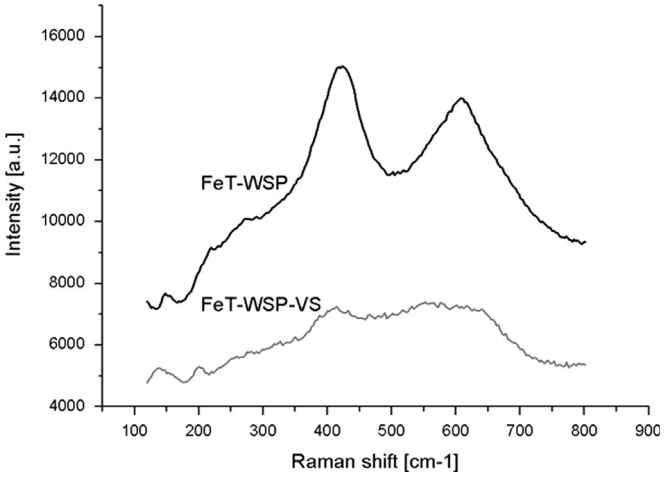

Fig. 4. Raman spectra of the coatings – FeT-WSP and FeT-WSP–VS.

Table 3
Surface roughness of the coatings and the photocatalytic kinetic rate constant *k* (for 365 nm).

Coating	R_a	$R_{y\ max}$	Kinetic rate constant *k* [h^{-1}]
FeT-WSP	14.0 ± 0.5	105.2 ± 1.8	0.1095
FeT-WSP–VS	23.8 ± 1.5	168.2 ± 6.7	0.2117
FeT-GSP	7.4 ± 0.7	56.2 ± 5.7	0.3121
R	*	*	0.0147

*Sample *R* was too soft for a contact technique measurement

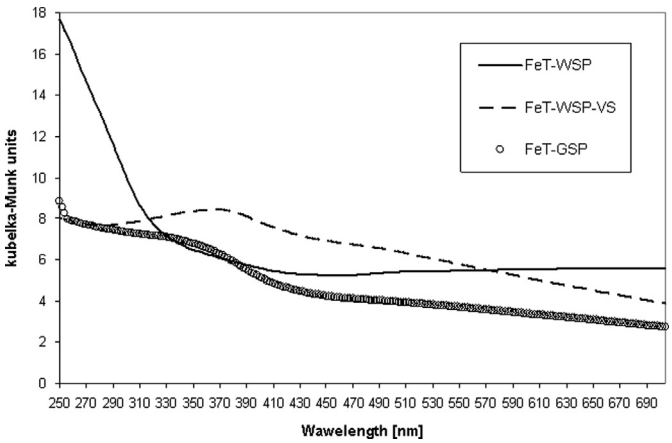

Fig. 5. Energetic comparison of the transfer of an electron from the valence band to the conduction band for all coatings – FeT-WSP, FeT-WSP–VS, and FeT-GSP.

visible light wavelength of 400 nm, FeT-GSP coating has a lower value than that of the FeT-WSP coating. The spectra do not drop sharply in the wavelength range of 340–400 nm, but a high *K–M* absorbance continues to longer wavelengths, especially for the FeT-WSP–VS coating. This is a consequence of an interaction of the metal ions (in our case Fe) with the TiO_2 catalyst [22,23]. The explanation is that more irradiation light energy of a broad-band source can be utilized. At the plasma spray process, also a few Fe_2O_3 powder reacted with TiO_2 powder and produced iron titanium oxide compounds, such as $FeTiO_3$, which may improve the photo-absorptive ability of the coatings in the visible spectral range [24]. Therefore, it is concluded that the photocatalytic activity of the FeT-WSP and FeT-WSP–VS coatings partly results from the absorbance of $FeTiO_3$. Na_2SiO_3 in the FeT-WSP–VS coating (without $FeTiO_3$) helps to stabilize the structural disorder most probably due to the Ti–O–Si chemical bonds [13]. Reported Fe-doped TiO_2 films [25,26] exhibited slight red-shift in absorbance and enhanced absorbance in the visible-light region compared with undoped TiO_2, attributed to a band gap narrowing by Fe^{3+} doping into TiO_2 [27], which is also supported by calculations [28]. The charge-transfer transition between dopant ions via the conduction band ($Fe^{3+}+Fe^{3+} \rightarrow Fe^{4+}+Fe^{2+}$) is mentioned as responsible for such behavior [26].

Extremely hydrogen-rich atmosphere at GSP spraying of the FeT powder led to the further continuation of the reactions (1) and (2) to complete reduction of certain amount of iron oxides to metallic iron.

Ilmenite $FeTiO_3$ is a semiconductor with a band gap of about 2.6 eV [29] and conduction band (CB) energy edge of 2.6 eV, approximating to that of TiO_2 (2.7 eV). Upon the irradiation of visible light (Vis), the electrons in the valence band (VB) of $FeTiO_3$ are excited to CB. Thus, the VB of $FeTiO_3$ becomes partly vacant; consequently, electrons in VB of TiO_2 can be transferred to that of $FeTiO_3$ due to their similarity in energy level, leaving behind the holes in VB of TiO_2. On the other hand, when the material is irradiated by UV–vis light, electrons in VB of TiO_2 are excited to CB which can be transferred to CB of $FeTiO_3$ because the flat-band potential of TiO_2 is 0.53 V higher than that of $FeTiO_3$. Consequently, electron–hole pairs are well-separated and electrons on ilmenite surface have sufficient lifetime for the reaction with a pollutant. Therefore, the photoactivity improvement along with increasing content of $FeTiO_3$ in the mixed $FeTiO_3$–TiO_2 system is expectable.

3.3. Photocatalysis

Concerning the photocatalytic degradation of butane, its concentration as well as reaction products – carbon dioxide and carbon monoxide – concentrations were detected at retention times of up to 24 h, see Figs. 6–8. The kinetic mechanism follows a pseudo-first-order equation, which can be expressed by the Langmuir–Hinshelwood kinetic model [30]. The rate constants are displayed in the last column of Table 3.

Under the UV light, among all coatings a complete degradation of butane is maintained after 24 h, but the kinetics of individual coatings differs with FeT-GSP being the fastest catalyst and FeT-WSP the slowest one; see Fig. 6a. The CO_2 uptake was relatively similar for FeT-WSP and FeT-WSP–VS, and at the same time for FeT-GSP it is significantly lower, as indicated in Fig. 7a. The CO uptake was also relatively similar for FeT-WSP and FeT-WSP–VS, whereas for FeT-GSP it is again significantly lower as seen in Fig. 8a.

Under visible light, the butane conversion, Fig. 6b, on the FeT-WSP–VS coating reached about 90% of butane decomposition, whereas both FeT coatings, i.e. WSP and GSP, reached a constant level of butane decomposition close to 100%. The GSP coating, as the best one, reached 100% even after 10 h. The CO_2 uptake for FeT-WSP–VS coating is markedly higher than under UV light. Both FeT-WSP coatings exhibit similar level of CO_2 creation as under UV light, whereas for FeT-GSP it is again markedly lower, c.f. Fig. 7b. And finally, the same statement could be repeated for carbon monoxide uptake, Fig. 8b.

So, the most effective photocatalyst is FeT-GSP, followed by FeT-WSP and FeT-WSP–VS, which is spectrally sensitive and responds well only under UV light. FeT-GSP and partly also FeT-WSP are able to degrade butane effectively at UV as well as visible light and produce relatively low quantity of CO and CO_2, toxic and environmentally problematic gases, respectively. We can speculate that part of the carbon from butane is incorporated in water in the form of carbonic acid H_2CO_3 [31].

The FeT-WSP–VS coating is predominantly amorphous but its photoactivity was higher than that of the anatase reference *R* sample, especially at visible light. In [32] it was shown that a sample with a limited crystallinity was a better photocatalyst than other, more crystalline samples. Also FeT-WSP and FeT-GSP coatings provide a better photoactivity than the TiO_2 reference *R* sample because of mechanisms mentioned in case of Ti-doped α-Fe_2O_3-based films [33]. The anatase crystallite size is smaller for the FeT-GSP coating compared to FeT-WSP coating. According to the literature, the small crystallite size can enhance the photoactivity of the TiO_2-based coatings [34].

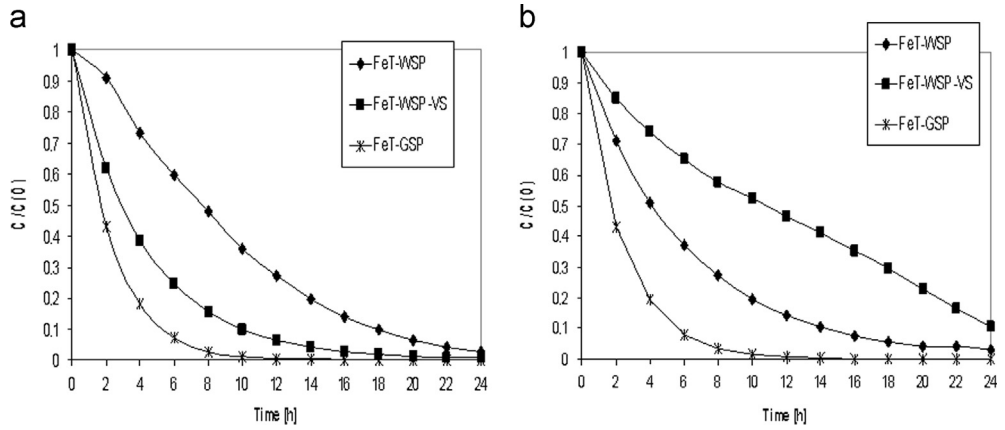

Fig. 6. Photocatalytic decomposition of butane under UV 365 nm (a) and visible light 400 nm (b).

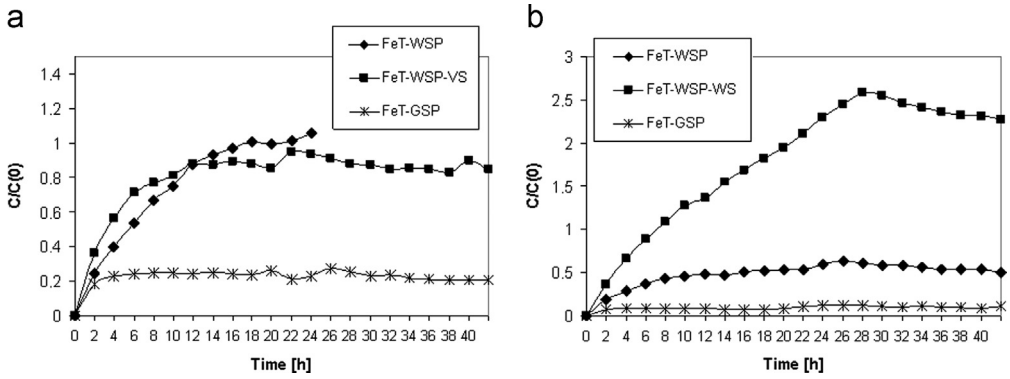

Fig. 7. Concentration growth of the reaction product – carbon dioxide under UV 365 nm (a) and visible light 400 nm (b).

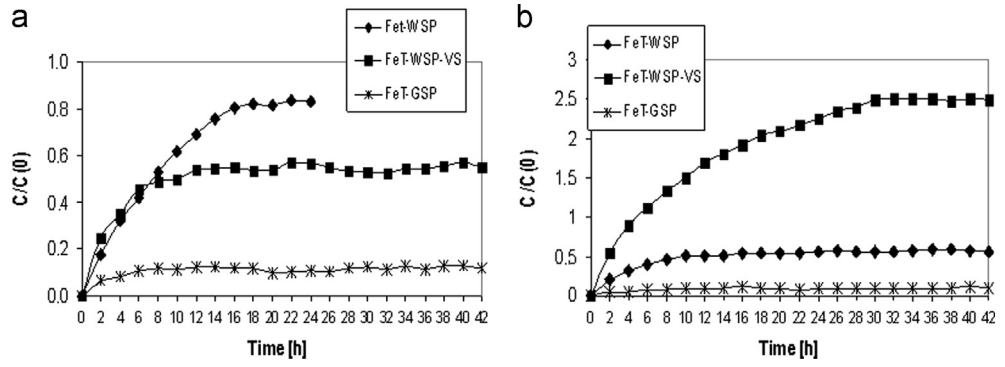

Fig. 8. Concentration growth of the reaction product – carbon monoxide under UV 365 nm (a) and visible light 400 nm (b).

4. Conclusions

The goal of this study was to examine the photocatalytic activity of coatings produced by atmospheric plasma spraying. The plasma guns used were gas- and water- stabilized; TiO_2–Fe_2O_3 powder with and without Na_2SiO_3 additive was agglomerated into particles suitable for plasma spraying.

Anatase titania from the feedstock powder was converted into rutile phase whereas a presence of $FeTiO_3$ was detected in the WSP coating without Na_2SiO_3. The coating from powder with Na_2SiO_3 was partly amorphous. All here addressed coatings were more photocatalytically active than a reference TiO_2 sample without Fe. At the WSP spray procedure, some Fe_2O_3 powder reacted with TiO_2 powder and produced ilmenite $FeTiO_3$. The coating with Na_2SiO_3 admixture have even finer anatase crystallites and a large amorphous portion, however its photoactivity was lower, whereas both coatings without Na_2SiO_3 admixture catalyzed the butane decomposition with high efficiency due to the advantageous inter-semiconductor hole-transfer mechanism. Extremely hydrogen-rich atmosphere at GSP spraying led to the complete reduction of certain amount of iron oxides to metallic iron. A charge-transfer transition between dopant ions via the conduction band took place in this coating, leading to the most efficient butane conversion under UV and also visible light.

Acknowledgments

This work was supported by the the Grant Agency of the Academy of Sciences of the Czech Republic (Project no. IAAX00430803).

References

[1] R. Molinari, F. Pirillo, M. Falco, V. Loddo, L. Palmisano, Photocatalytic degradation of dyes by using a membrane reactor, Chemical Engineering Processes 43 (2004) 1103–1114.
[2] N. Serpone, I. Texier, A.V. Emeline, P. Pichat, H. Hidaka, J. Zhao, Post-irradiation effect and reductive dechlorination of chlorophenols at oxygen-free TiO_2/water interfaces in the presence of prominent hole scavengers, Journal of Photochemical and Photobiological Sciences A–Chemical 136 (2000) 145–155.
[3] M.C. Canela, R.M. Alberici, R.C.R. Sofia, M.N. Eberlin, W.F. Jardim, Destruction of malodorous compounds using heterogeneous photocatalysis, Environmental Science and Technology 33 (1999) 2788–2792.
[4] S. Boukrouh, R. Bensaha, S. Bourgeois, E. Finot, M.C. Marco de Lucas, Reactive direct current magnetron sputtered TiO_2 thin films with amorphous to crystalline structures, Thin Solid Films 516 (2008) 6353–6358.
[5] Y. Ju, L. Li, Z. Wu, Y. Jiang, Effect of oxygen partial pressure on the optical property of amorphous titanium oxide thin films, Energy Procedia 12 (2011) 450–455.
[6] F.X. Ye, T. Tsumura, K. Nakata, A. Ohmori, Dependence of photocatalytic activity on the compositions and photo-absorption of functional TiO_2–Fe_3O_4 coatings deposited by plasma spray, Materials Science and Engineering B 148 (2008) 154–161.
[7] F.X. Ye, A. Ohmori, The photocatalytic activity and photo-absorption of plasma sprayed TiO_2–Fe_3O_4 binary oxide coatings, Surface and Coatings Technology 160 (2002) 62–67.
[8] F.X. Ye, A. Ohmori, Ch. Li, New approach to enhance the photocatalytic activity of plasma sprayed TiO_2 coatings using p–n junctions, Surface and Coatings Technology 184 (2004) 233–238.
[9] Y.J. Kim, B. Gao, S.Y. Han, M.H. Jung, A.K. Chakraborty, T. Ko, Ch. Lee, W.I. Lee, Heterojunction of $FeTiO_3$ nanodisc and TiO_2 nanoparticle for a novel visible light photocatalyst, Journal of Physical Chemistry C 113 (44) (2009) 19179–19184.
[10] R.S. Lima, B.R. Marple, From APS to HVOF spraying of conventional and nanostructured titania feedstock powders: a study on the enhancement of the mechanical properties, Surface and Coatings Technology 200 (2006) 3428–3437.
[11] M. Bozorgtabar, M. Rahimipour, M. Salehi, M. Jafarpour, Structure and photocatalytic activity of TiO_2 coatings deposited by atmospheric plasma spraying, Surface and Coatings Technology 205 (2011) 229–231.
[12] P. Ctibor, M. Hrabovsky, Plasma sprayed TiO_2, the influence of power of an electric supply on particle parameters in the flight and character of sprayed coating, Journal of the European Ceramic Society 30 (2010) 3131–3136.
[13] H. Zheng, Ch. Wang, A. Zhang, L. Zhang, S. Xia, Z. Zhao, Effect of Na_2SiO_3 on synthesis of TiO_2 nanopowders by thermal processing of the precursor, Advanced Powder Technology 22 (2011) 581–586.
[14] M.A. Rahman, S. Kaneco, T. Suzuki, H. Katsumata, K. Ohta, A.M. Shafiqul Alam, Development of sintering materials by sea sediments and TiO_2 for the cleaning technology, Pakistanian Journal of Analytical and Environmental Chemistry 8 (1–2) (2007) 26–35.
[15] V. Stengl, V. Houskova, S. Bakardjieva, N. Murafa, Photocatalytic degradation of acetone and butane on mesoporous titania layers, New Journal of Chemistry 34 (2010) 1999–2005.
[16] A.A. Christy, O.M. Kvalheim, R.A. Velapoldi, Quantitative analysis in diffuse reflectance spectrometry: a modified Kubelka–Munk equation, Vibrational Spectroscopy 9 (1995) 19–27.
[17] P. Ctibor, H. Ageorges, V. Stengl, N. Murafa, I. Pis, T. Zahoranova, V. Nehasil, Z. Pala, Structure and properties of plasma sprayed $BaTiO_3$ coatings: spray parameters versus structure and photocatalytic activity, Ceramics International 37 (2011) 2561–2567.
[18] X.H. Wang, J.-G. Li, H. Kamiyama, T. Ishigaki, Fe-doped TiO_2 nanopowders by oxidative pyrolysis of organometallic precursors in induction thermal plasma: synthesis and structural characterization, Thin Solid Films 506–507 (2006) 278–282.
[19] I.N. Martyanov, T. Berger, O. Diwald, S. Rodrigues, K.J. Klabunde, Enhancement of TiO_2 visible light photoactivity through accumulation of defects during reduction–oxidation treatment, Journal of Photochemistry and Photobiology A: Chemistry 212 (2010) 135–141.
[20] S. Kumar, V. Selvarajan, P.V.A. Padmanabhan, K.P. Sreekumar, Spheroidization of metal and ceramic powders in thermal plasma jet: comparison between experimental results and theoretical estimation, Journal of Materials Processing Technology 176 (2006) 87–94.
[21] T.D. Robert, L.D. Laude, V.M. Geskin, R. Lazzaroni, R. Gouttebaron, Micro-Raman spectroscopy study of surface transformations induced by excimer laser irradiation of TiO_2, Thin Solid Films 440 (2003) 268–277.
[22] M. Anpo, Use of visible light, second-generation titanium oxide photocatalysts prepared by the application of an advanced metal ion-implantation method, Pure and Applied Chemistry 72 (9) (2000) 1787–1792.
[23] J.-M. Huang, Y.-X. Li, G.-D. Zhao, X.-P Cai, Photocatalytic degradation characteristic of amorphous TiO_2-W thin films deposited by magnetron sputtering, Transactions of Nonferrous Metals Society of China 16 (2006) 280–284.
[24] N. Smirnova, A. Eremenko, O. Rusina, W. Hopp, L. Spanhel, Synthesis and characterization of photocatalytic porous Fe^{3+}/TiO_2 layers on glass, Journal of Sol–Gel Science and Technology 22 (2001) 109–113.
[25] Z. Li, W. Shen, W. He, X. Zu, Effect of Fe-doped TiO_2 nanoparticle derived from modified hydrothermal process on the photocatalytic degradation performance on methylene blue, Journal of Hazardous Materials 155 (2008) 590–594.
[26] J.A. Navio, G. Colon, M.I. Litter, G.N. Bianco, Synthesis, characterization and photocatalytic properties of iron-doped titania semiconductors prepared from TiO_2 and iron (III) acetylacetonate, Journal of Molecular Catalysis A: Chemical 106 (1996) 267–276.
[27] T.K. Ghorai, M. Chakraborty, P. Pramanik, Photocatalytic performance of nano-photocatalyst from TiO_2 and Fe_2O_3 by mechanochemical synthesis, Journal of Alloys and Compounds 509 (2011) 8158–8164.
[28] D.V. Wellia, Q.C. Xu, M.A. Sk, K.H. Lim, T.M. Lim, T.T. Yang Tan, Experimental and theoretical studies of Fe-doped TiO_2 films prepared by peroxo sol-gel method, Applied Catalysis A: General 401 (2011) 98–105.
[29] Q.D. Truong, J.-Y. Liu, C.-C. Chung, Y.-C. Ling, Photocatalytic reduction of CO_2 on $FeTiO_3$/TiO_2 photocatalyst, Catalysis Communications 19 (2012) 85–89.
[30] Y. Yang, Q. Wu, Y. Guo, C. Hu, E. Wang, Efficient degradation of dye pollutants on nanoporous polyoxotungstate – anatase composite under visible-light irradiation, Journal of Molecular Catalysis A 225 (2) (2005) 203–212.
[31] S. Mozia, Application of temperature modified titanate nanotubes for removal of an azo dye from water in a hybrid photocatalysis-MD process, Catalysis Today 156 (2010) 198–207.
[32] N.A. Jamalluddin, A.Z. Abdullah, Reactive dye degradation by combined Fe (III)/TiO_2 catalyst and ultrasonic irradiation: effect of Fe(III) loading and calcination temperature, Ultrasonics Sonochemistry 18 (2011) 669–678.
[33] G. Wang, Y. Ling, D.A. Wheeler, K.E.N. George, K. Horsley, C. Heske, J.Z. Zhang, Y. Li, Facile synthesis of highly photoactive α-Fe_2O_3-based films for water oxidation, Nano Letters 11 (2011) 3503.
[34] Ch. Lee, H. Choi, Ch. Lee, H. Kim, Photocatalytic properties of nanostructured TiO_2 plasma sprayed coating, Surface and Coatings Technology 173 (2003) 192.